CrossMark

# Pathways to Dissipation in Weakly Collisional Plasmas

William H. Matthaeus[1] , Yan Yang[2,3] , Minping Wan[2], Tulasi N. Parashar[1] , Riddhi Bandyopadhyay[1] ,
Alexandros Chasapis[1], Oreste Pezzi[4,5] , and Francesco Valentini[6]

[1] Bartol Research Institute, Department of Physics and Astronomy, University of Delaware, Newark, DE, USA
[2] Southern University of Science and Technology, Shenzhen, Guangdong 518055, People's Republic of China
[3] University of Science and Technology of China, Hefei, Anhui 230026, People's Republic of China
[4] Gran Sasso Science Institute, Viale F. Crispi 7, I-67100 LAquila, Italy
[5] INFN/Laboratori Nazionali del Gran Sasso, Via G. Acitelli 22, I-67100 Assergi (AQ), Italy
[6] Department of Physics, University of Calabria, Rende, Italy

## Abstract

Observed turbulence in space and astrophysics is expected to involve cascade and subsequent dissipation and heating. Contrary to standard collisional fluid turbulence, the weakly collisional magnetized plasma cascade may involve several channels of energy conversion, interchange, and spatial transport, leading eventually to the production of internal energy. This paper describes these channels of transfer and conversion, collectively amounting to a complex generalization of the Kolmogorov cascade. Channels may be described using compressible magnetohydrodynamic (MHD) and multispecies Vlasov–Maxwell formulations. Key steps are conservative transport of energy in space, parallel incompressible and compressible cascades in scale, electromagnetic work on particles driving macroscopic and microscopic flows, and pressure–strain interactions, both compressive and shear-like, that produce internal energy. A significant contrast with the collisional case is that the steps leading to the disappearance of large-scale energy in favor of internal energy are formally reversible. This property motivates a discussion of entropy, reversibility, and the relationship between dissipation with collisions and in the Vlasov system without collisions. Where feasible, examples are given from MHD and Particle in Cell simulations and from *MMS* observations.

## 1. Introduction

In standard turbulence theory for a collisional medium, the cascade transfers energy from large scale to small scale where viscosity and resistivity remove fluctuation energy in favor of heat. In weakly collisional plasmas, such as the solar wind, solar corona, or terrestrial magnetosheath, a cascade is observed, and heating occurs, but through what mechanisms? Detailed observation (Cranmer 2009; Matthaeus & Velli 2011; Bruno & Carbone 2013) and supporting simulations (Daughton et al. 2011a; Karimabadi et al. 2013) indicate that dissipation of turbulent fluctuations makes important contributions to heating, transport, and particle energization in solar and heliospheric environments (Zank et al. 1996, 2014). There have been various efforts to describe this dissipation as occurring due to specific wave modes and instabilities, or through specific physical mechanisms such as reconnection, phase mixing, or stochastic heating. Another approach, reviewed and developed in the present paper, describes the channels for energy transfer across scales, and for conversion from one form to another, leading eventually to heating and dissipation. Instead of identifying specific mechanisms, the pathways for energy transfer are identified, and then quantified, without resorting to simplifying assumptions that accompany the identification of specific dominant mechanisms. All available channels, apart from collisions, are formulated based on the multispecies Vlasov equation. Therefore, an identification of a dominant pathway to dissipation necessarily includes all mechanisms that are consistent with that description. We offer the viewpoint that the description of transfer and conversion channels, even if less familiar in space plasma physics, is a potentially direct and

compact approach to problems such as plasma dissipation. Such an effort is well supported by modern simulation tools and observational instruments that are capable of quantifying all of the terms that contribute to these pathways.

## 2. Mechanisms and Pathways in Turbulence

In plasma physics, candidate dissipation mechanisms are often based on linear Vlasov theory. In this approach, largely based on laboratory plasma studies, solutions for perturbations about an assumed equilibrium give rise to wave modes, damping rates, and instabilities. A typical strategy might consist of identifying the correct instability or wave that accounts for specific observed features of interest. In the laboratory context, the calculation of the correct eigenmode or fastest growing unstable mode might give insight into the failure mode of a plasma discharge. A similar approach is frequently adopted in identifying mechanisms in space physics.

Linear theory may also be extended into weak turbulence theory, in which nonlinearities are computed as a higher-order correction. An even deeper extension, the "wave turbulence" perspective, assumes that strong turbulence states remain decomposable in terms of the linear eigenstates.

Mechanisms relevant to dissipation might also be fully nonlinear but simple enough to be useful paradigms. A familiar example is magnetic reconnection, a mechanism frequently invoked for the release of energy stored in magnetic fields and as a source of suprathermal particles. Different perspectives exist—it has been argued recently (Mallet et al. 2017) that reconnection modifies the cascade, in contrast to the earlier

suggestion (Matthaeus & Lamkin 1986) that reconnection is essential in order to have a cascade in a magnetized plasma or magnetofluid.

A contrasting perspective is that strong turbulence is not well characterized by equilibria. The dispersion relations needed to define eigenstates may be only rarely realized. Even if (near-) equilibria are formed, for example, relaxation processes (Servidio et al. 2008b), these are likely nonuniform, and it may be very difficult to quantitatively define those states. Furthermore, attempts to identify an isolated dissipative mechanism that operates within turbulence could be over-optimistic, as it is quite possible that many individual processes may be operating. For example, in the high-resolution, shear-driven, strongly turbulent simulation described by Karimabadi et al. (2013), one can clearly identify Alfvén waves, reconnection, linear tearing, Kelvin–Helmholtz, compression, and other contributing mechanisms. However, in describing such complex dynamics, one tends to rely more on ideas developed from hydrodynamics, such as the notion of the Kolmogorov cascade (to be described below), that produce different types of simplification, many of which are statistical rather than deterministic.

A standard view of turbulence, whether in hydrodynamics or magnetohydrodynamics, or in a weakly collisional plasma, is that available energy resides at large scales, and through nonlinear interactions, this energy is transferred through an intermediate inertial range of scales into small scales where dissipation occurs (Orszag 1977). This nonlinear energy cascade has numerous influences on the macroscopic and thermal properties of heliospheric plasmas, in that it contributes to the heating of the solar corona, the origin of the solar wind, and numerous other space physics problems (Matthaeus & Velli 2011). In collisionless plasmas, the scattering and energization of charged particles often depends sensitively on turbulence properties (Jokipii 1966; Shalchi 2009), so that turbulence can be a controlling factor in suprathermal particle and energy transport in space and astrophysics. Similar physical effects are broadly relevant in astrophysical plasmas (Lazarian et al. 2012), where turbulence plays a role in the dynamics of molecular clouds and star formation (Mac Low 1999), and in cooling flows where turbulence regulates heat transport (Chandran & Cowley 1998; Banerjee & Sharma 2014).

For a kinetic plasma, the theoretical understanding is less developed and perhaps more controversial, but there is also accumulating evidence that large-scale reservoirs of energy regulate the rate of relaxation, fueling the plasma physics response at very much smaller scales, leading eventually to dissipation (Karimabadi et al. 2013).

The classical cascade scenario often features a power-law inertial range spectrum that describes a spectral distribution of energy across scales. Of equal importance is that the inertial range acts as a near-lossless conduit that connects energy-containing large scales to the dissipative small scales. This energy transfer across scales in effect "completes" the circuit that allows a system far from equilibrium to relax toward thermal equilibrium. In sufficiently large hydrodynamic and MHD systems, it is widely recognized that the energy-containing eddies control the rate of transfer into the inertial range and therefore control the dissipation rate, on average. In the following sections, we will be examining how the turbulence cascade in collisionless plasma becomes more complex than the von Karman–Kolmogorov picture, simply because there are more channels available for energy transport and conversion. As a first step, we review the salient features of the standard Kolmogorov 1941 cascade picture.

## 3. Simple Cascade and First Level of Complexity due to Compressions

A von Karman–Howarth picture of turbulent decay (de Kármán & Howarth 1938) may be adapted for MHD (Hossain et al. 1995; Wan et al. 2012). A similarity-law decay rate, written in terms of the Elsässer amplitudes $Z_+$ and $Z_-$ and their respective similarity length scales $\lambda_+$ and $\lambda_-$, may be written as $\epsilon = \epsilon_+ + \epsilon_-$ with $\epsilon_\pm \equiv C_\pm Z_\pm^2 Z_\mp / \lambda_\pm$. The constants $C_\pm$ may depend on other parameters. A recent study (Bandyopadhyay et al. 2018b) examined the behavior of the constants $C_\pm$ for varying Reynolds numbers and mean magnetic field strengths. A simplified version, accurate when normalized cross-helicity $\sigma_c = (Z_+^2 - Z_-^2)/(Z_+^2 + Z_-^2)$ is small, is $\epsilon \approx C_K \frac{Z^3}{\lambda}$ in terms of a single correlation scale $\lambda$, a single von Karman constant $C_K$, and total fluctuation strength $Z^2 = Z_+^2 + Z_-^2$.

Upon examining the scale (or wavenumber) decomposition of the fluctuations, one may argue, based on the symmetries of the problem, that a self-similar cascade might be local in scale so that statistical properties at a given scale might depend only on that scale $\ell$ and the rate of energy transfer across scales $\epsilon$. Ignoring nonsteady fluctuations and intermittency, and other complications, the decay rate $\epsilon$ enters the expression for the steady inertial range spectrum,

$$\mathcal{E}(k) = C\epsilon^{2/3}k^{-5/3}. \tag{1}$$

This spectral law is the basic content of the Kolmogorov 1941 theory (K41). It is, strictly speaking, appropriate to isotropic incompressible hydrodynamics at high Reynolds number, but is more widely applied as a baseline description of turbulence. For example, with suitable simplifications, the same reasoning is expected to hold also for incompressible MHD.

If one adds to this picture an accommodation for nonuniform dissipation, then the dissipation function becomes a random function of position $\epsilon \to \epsilon(\boldsymbol{x})$. In the Kolmogorov (1962, hereafter K62) picture, this forms the basis of intermittency and the emergence of coherent structures, while only slightly modifying the isotropic spectral law. This view of turbulence cascade is the template for what we refer to here as the simple cascade picture, which is illustrated in Figure 1.

*Third-order law and complexity.* Attaining a direct cascade from large to small scales is not quite as simple as suggested in the above picture. Even though the incompressible cascade is approximately local in scale, there is some degree of nonlocality (Verma et al. 2005; Alexakis 2007; Alexakis et al. 2007). Furthermore scale to scale transfer occurs in both forward and reverse directions, with a slight preponderance of large- to small-scale transfer. This is manifestly seen in the statistical distributions leading to Kolmogorov's third-order law (Kolmogorov 1941a; Taylor et al. 2003). Individual estimates of the cubed longitudinal increment $\delta u_\ell^3$ are almost equally likely to be negative or positive. But in the ensemble average sense, there is a definite sign and $\langle \delta u_\ell^3 \rangle = -\frac{4}{5}\epsilon\ell$ (Pope 2000). For this reason, one expects that estimates of all types of energy transfer (scale-to-scale, sharp Fourier, third order, etc.) will exhibit large fluctuations (Verma et al. 2005;
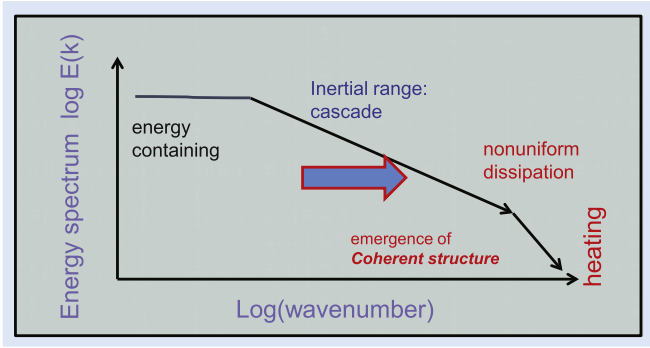
**Figure 1.** Simple cascade diagram based on incompressible equations and depicting only the average scale transfer. Intermittency emerges even in this simple picture.

Coburn et al. 2015), with the direct cascade emerging only after suitable averaging.

In incompressible MHD, the energy cascade within the inertial range satisfies the Politano–Pouquet law (Politano & Pouquet 1998):

$$S_{\parallel}^{\pm}(r) = \langle \delta z_{\parallel}^{\mp} \delta z_i^{\pm} \delta z_i^{\pm} \rangle = -\frac{4}{d}\epsilon^{\pm}r, \qquad (2)$$

where $z^{\pm} = u \pm b/\sqrt{4\pi\rho}$, $\delta z^{\pm} = z^{\pm}(x+r) - z^{\pm}(x)$, $\delta z_{\parallel}^{\pm} = \delta z^{\pm} \cdot r/r$, $\epsilon^{\pm}$ is the mean energy transfer rate, and $d$ is the spatial dimension. The average total energy transfer rate is defined as $\epsilon = (\epsilon^{+} + \epsilon^{-})/2$. Recently, the unaveraged third-order mixed structure function has been used in applications (Sorriso-Valvo et al. 2018a, 2018b) as a surrogate of the local-in-position energy transfer rate (LET). We denote by $\epsilon_r^{\pm}$ the "local" pseudo-energy transfer rate at the scale $r$,

$$\epsilon_r^{\pm} = -\frac{d}{4}\frac{\delta z_{\parallel}^{\mp} \delta z_i^{\pm} \delta z_i^{\pm}}{r}, \qquad (3)$$

so that the LET is computed as

$$\epsilon_r = \frac{\epsilon_r^{+} + \epsilon_r^{-}}{2}. \qquad (4)$$

The averaged third-order structure functions (see Equation (2)) are shown in Figure 2, for both kinetic simulation (see Appendix A) and for magnetosheath observations by the *MMS* spacecraft. In both cases, the turbulence being described is in a weakly compressive regime, and the scales examined are those thought to be well described by MHD. Such results represent a quantitative evaluation of the average energy transfer through the incompressible cascade channel. Fluctuations in this channel, and the behavior of additional channels of energy transfer and conversion, are discussed in Section 5.

*Compressibility adds a new channel.* When incompressibility is relaxed, the internal energy becomes another new element in the turbulence energy balance. While the incompressible channel remains available, an additional contribution to energy transfer emerges, the so-called pressure dilatation $p\nabla \cdot u$. The relationship between compressible and incompressible turbulence has been studied in a variety of approaches, including formal analysis (Klainerman & Majda 1981), asymptotic perturbation theory (Zank & Matthaeus 1991), and scale filtering (Eyink 2005; Aluie 2011), as well as in MHD (Zank & Matthaeus 1993; Yang et al. 2016; Andrés et al. 2018; Hadid et al. 2018; Hellinger et al. 2018).
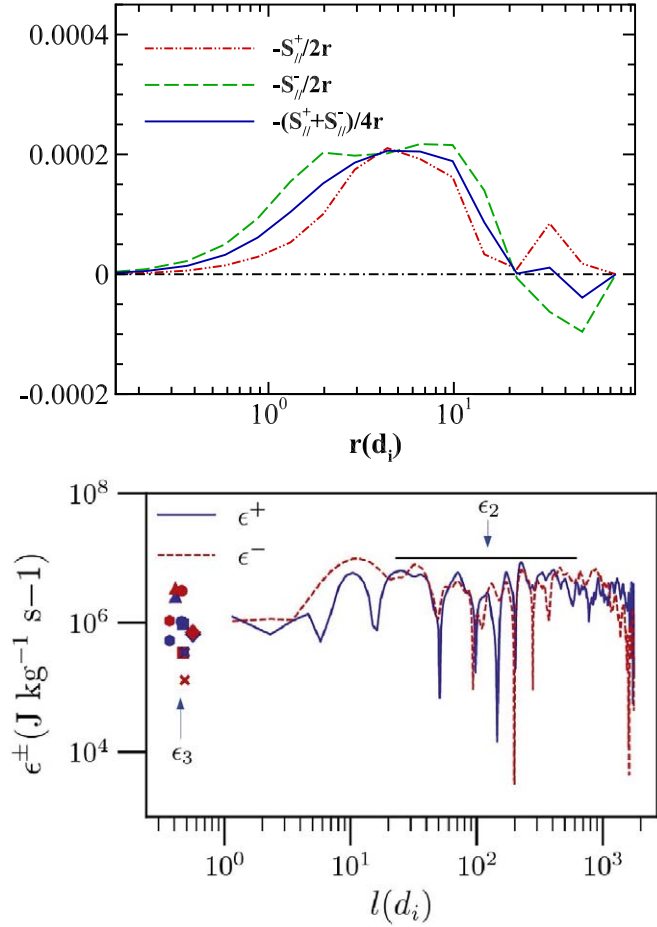




**Figure 2.** Estimates of transfer rate as a function of scale for the MHD-like cascade, extended into the kinetic range, showing attenuation of this channel at subproton scales. (Top) Results from a 2.5D kinetic PIC simulation. See Yang et al. (2019) and Appendix A. (Bottom) Results from *MMS* data analysis in the terrestrial magnetosheath. Lines are computed from single spacecraft analysis using the Taylor hypothesis. Symbols are two spacecraft estimates using pairs of *MMS* spacecraft. See Bandyopadhyay et al. (2018a).
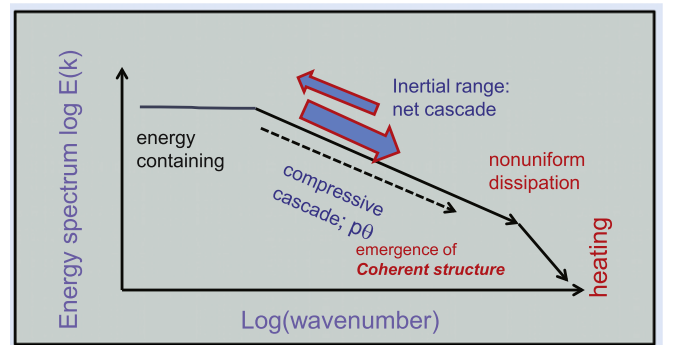


**Figure 3.** A more complex cascade diagram, including bidirectional scale-to-scale transfers, possible nonlocality, and compressional effects.

An interesting recently discovered feature is that the net transfer into pressure dilatation saturates at small scales, so that the incompressible and compressible cascades decouple at smaller scales (Aluie 2011; Aluie et al. 2012). This provides justification for treating the kinetic energy as a cascaded quantity, although it is not formally conserved by compressible nonlinear interactions. A diagram suggesting the increased complexity of a compressible cascade is shown in Figure 3.

## 4. Multiple Channels of Energy Transfer and Conversion

In obtaining fluid models such as hydrodynamics or MHD, collisions are important because they rapidly produce an isotropic pressure tensor, and in the Chapman–Enskog limit of strong collisions, the even stronger condition of Local Thermodynamic Equilibrium (LTE). However in the opposite limit, widely applicable in space and astrophysical plasmas, collisions are weak or absent. Then we consider a collisionless plasma consisting of species labeled by $\alpha$ to be described by the Vlasov equations,

$$\partial_t f_\alpha + \boldsymbol{v} \cdot \nabla f_\alpha + \frac{q_\alpha}{m_\alpha}\left(\boldsymbol{E} + \frac{\boldsymbol{v}}{c} \times \boldsymbol{B}\right) \cdot \nabla_v f_\alpha = 0. \quad (5)$$

These are coupled to the Maxwell equations that determine the electromagnetic fields. We will be particularly concerned below with the energy budgets of the particles and fields, and the physical quantities that contribute to their time variations.

We will examine the energy budget of a weakly collisional plasma, and the manner in which turbulence influences it, leading to transfer from energy-containing large scales, and in analogy to the treatment of fluid cascades discussed above, through intermediate scales, and eventually into heat or internal energy. The total energy density at position $\boldsymbol{x}$ and time $t$ is the sum of the electromagnetic energy density,

$$\mathcal{E}^m(\boldsymbol{x}, t) = \frac{1}{8\pi}(\boldsymbol{B}^2(\boldsymbol{x}, t) + \boldsymbol{E}^2(\boldsymbol{x}, t), \quad (6)$$

and the sum over species of the individual particle kinetic energy densities,

$$\mathcal{E}_\alpha = \frac{1}{2}m_\alpha \int |\boldsymbol{v}|^2 f_\alpha(\boldsymbol{x}, \boldsymbol{v}, t)d\boldsymbol{v}. \quad (7)$$

Here, $\boldsymbol{B}$ and $\boldsymbol{E}$ are magnetic and electric fields, respectively, $m_\alpha$ is the mass of particles of species $\alpha$, and $f_\alpha$ is the velocity distribution function (vdf) of particles of type $\alpha$, varying in position and time.

The collective motion is quantified by the fluid velocity $\boldsymbol{u}_\alpha$ defined by

$$n_\alpha \boldsymbol{u}_\alpha = \int \boldsymbol{v} f_\alpha d\boldsymbol{v}, \quad (8)$$

where $n_\alpha = \int f_\alpha d\boldsymbol{v}$ is the number density of species $\alpha$. We refer to the above energy densities, for brevity, simply as energies.

Separating the kinetic energy into the contribution due to the fluid motion, and the remainder, which we call the internal energy, is essential for understanding the energy conversion processes. The fluid flow kinetic energy of species $\alpha$ is

$$\mathcal{E}_\alpha^f = \frac{1}{2}\rho_\alpha|\boldsymbol{u}_\alpha|^2, \quad (9)$$

and the corresponding internal energy is

$$\mathcal{E}_\alpha^{\text{th}} = \frac{1}{2}m_\alpha \int (\boldsymbol{v} - \boldsymbol{u}_\alpha)^2 f_\alpha(\boldsymbol{x}, \boldsymbol{v}, t)d\boldsymbol{v}. \quad (10)$$

It is obvious that $\mathcal{E}_\alpha = \mathcal{E}_\alpha^f + \mathcal{E}_\alpha^{\text{th}}$.

The time evolution of the energies follows directly from standard elementary manipulations of the Vlasov equation and Maxwell equations. The fluid flow energy evolves in time according to

$$\partial_t \mathcal{E}_\alpha^f + \nabla \cdot (\mathcal{E}_\alpha^f \boldsymbol{u}_\alpha) + \nabla \cdot (\boldsymbol{P}_\alpha \cdot \boldsymbol{u}_\alpha)$$
$$= (\boldsymbol{P}_\alpha \cdot \nabla) \cdot \boldsymbol{u}_\alpha + n_\alpha q_\alpha \boldsymbol{u}_\alpha \cdot \boldsymbol{E}. \quad (11)$$

Similarly, one obtains the time evolution equation for the internal kinetic energy of species $\alpha$,[7]

$$\partial_t \mathcal{E}_\alpha^{\text{th}} + \nabla \cdot (\mathcal{E}_\alpha^{\text{th}} \boldsymbol{u}_\alpha) + \nabla \cdot \boldsymbol{h}_\alpha$$
$$= -(\boldsymbol{P}_\alpha \cdot \nabla) \cdot \boldsymbol{u}_\alpha. \quad (12)$$

where $\boldsymbol{h}_\alpha$ is the heat flux vector.

Finally, using the Maxwell equations, the evolution of the energy $\mathcal{E}^m$ in the electromagnetic field is described as

$$\partial_t \mathcal{E}^m + \frac{c}{4\pi}\nabla \cdot (\boldsymbol{E} \times \boldsymbol{B}) = -\boldsymbol{J} \cdot \boldsymbol{E}. \quad (13)$$

Here, $\boldsymbol{J} = \sum_\alpha \boldsymbol{J}_\alpha$ is the total electric current density and $\boldsymbol{J}_\alpha = n_\alpha q_\alpha \boldsymbol{u}_\alpha$ is the electric current density of species $\alpha$.

Several features of Equations (11)–(13) must be emphasized. First, all the terms grouped with the time derivatives on the left-hand sides are transport terms that do not change the total amount of energy of the respective types, but simply relocate energy of a given type from one location to another. These transport terms integrate to zero for suitable boundary conditions and may be extremely important in reconciling the energy balance at any point in space and time. However, important as they may be in particular problems, we are less concerned with transport effects here, as the emphasis is on conversion between different types of energy.[8] Therefore, we will focus on the terms of these equations that are responsible for the conversion of energy from one form to another.

Examining the expressions on the right-hand side, it is evident that the term $\boldsymbol{J}_\alpha \cdot \boldsymbol{E}$ exchanges electromagnetic energy and flow energy for a species $\alpha$. All changes of internal ("thermal") energy of each species are accomplished exclusively by the pressure–strain interaction, which we abbreviate as $\text{PS}_\alpha \equiv -(\boldsymbol{P}_\alpha \cdot \nabla) \cdot \boldsymbol{u}_\alpha = -P_{ij}^{(\alpha)} \nabla_i u_j^{(\alpha)}$. The importance of pressure–strain interactions has been emphasized in a number of recent papers (Del Sarto et al. 2016; Yang et al. 2017a, 2017b, 2019; Chasapis et al. 2018; Pezzi et al. 2019b)

It should be emphasized that quantities such as $\boldsymbol{J}_\alpha \cdot \boldsymbol{E}$ and $\text{PS}_\alpha$ are not single-signed, as energy may be transferred into, or out of, the electromagnetic fields, and likewise, into or out of the collective fluid motion of each species $\alpha$. While the distributions of these quantities are not sign-definite, the expectation is that when there is net dissipation and heating, the appropriate sign indicating net transfer into random motions will be favored. This has been seen in magnetosheath observations (Retinò et al. 2007) and in plasma simulations in decaying turbulence (Wan et al. 2012; Yang et al. 2017a). Therefore, with some care, these quantities may be used to trace the flow of energy through different channels leading to dissipation. In fact, the evaluation of total $\boldsymbol{J} \cdot \boldsymbol{E}$ in the proton or

---

7 Some readers may prefer to use terminology such as "thermal energy" or "random kinetic energy" to refer to the quantity $\mathcal{E}_\alpha^{\text{th}}$.

8 Transport effects such as heat flux and convective heat transport are in many circumstances the dominant contributions to the balance of Equation (12); however, these terms do not exchange energy between different forms, and it is the exchange between different pathways or channels that is our main interest here.

electron fluid frames is often viewed as a "dissipation measure."[9]

Further decomposition of the pressure–strain term is convenient and physically revealing. A standard procedure for decomposing the pressure tensor $P_{ij}^{(\alpha)}$ and the stress tensor $S_{ij}^{(\alpha)} = \nabla_i u_j^{(\alpha)}$ is to separate out the trace. One then defines

$$P_{ij}^{(\alpha)} = p_\alpha \delta_{ij} + \Pi_{ij}^{(\alpha)}, \tag{14}$$

where $p_\alpha = \frac{1}{3} P_{jj}^{(\alpha)}$. Similarly, the stress tensor is conveniently decomposed as

$$S_{ij}^{(\alpha)} = \frac{1}{3} \theta_\alpha \delta_{ij} + D_{ij}^{(\alpha)} + \Omega_{ij}^{(\alpha)}, \tag{15}$$

where $\theta_\alpha = \nabla_i u_i^{(\alpha)}$ is the dilatation, and $D_{ij}^{(\alpha)} = \frac{1}{2}(\nabla_i u_j^{(\alpha)} + \nabla_j u_i^{(\alpha)}) - \frac{1}{3}\theta_\alpha \delta_{ij}$ and $\Omega_{ij}^{(\alpha)} = \frac{1}{2}(\nabla_i u_j^{(\alpha)} - \nabla_j u_i^{(\alpha)})$ are the symmetric and antisymmetric stress tensors, respectively. Then we see immediately that the pressure–strain interaction neatly separates as $PS_\alpha = -p_\alpha \theta_\alpha + PiD_\alpha$, where we have defined $PiD_\alpha \equiv -\Pi_{ij}^{(\alpha)} D_{ij}^{(\alpha)}$ and the antisymmetric stress $\Omega_{ij}^{(\alpha)}$ does not appear (Del Sarto et al. 2016).

*An aside: pressure–strain interaction in the collisional case.* The role of pressure–strain interaction in dissipation may seem at first unfamiliar to some readers, especially those with a plasma background, given that the term "dissipation" is often associated with the electromagnetic work on particles, $\mathbf{J} \cdot \mathbf{E}$, in many recent published works. However, it is not difficult to convince oneself that the pressure–strain interaction PS represents a critical channel leading to dissipation, even in ordinary gas dynamics. In fact, in collision-dominated gas dynamics, the usual procedure is to develop a Chapman–Enskog expansion in a small parameter, the Knudsen number.

One begins with a kinetic equation that is analogous to Equation (5), except that a collision operator $\Omega(f)$ is present in the right-hand side, which, following Boltzmann's assumptions, depends only on the one-body distribution $f(\mathbf{x}, \mathbf{v}, t)$. If the collisional mean free path $\lambda$ is much smaller than the scales $L$ over which the medium varies, i.e., the fluid scales, then we say that the medium is strongly collisional. Formally, in the Chapman–Enskog approach, one treats $\epsilon = \lambda/L$ as small, the collisions as strong and of order $\sim 1/\epsilon$. Then, the distribution is expanded $f = f^{(0)} + \epsilon f^{(1)} + \epsilon^2 f^{(2)} \dots$. In the perturbation hierarchy, at $O(\epsilon^{-1})$, the sole relation is $\Omega(f^{(0)}) = 0$, which locally forces the leading-order distribution to be a stationary state of the collision operator. In cases of interest, this is a local Maxwellian, with spatially varying density and temperature. If one then computes the familiar equations of evolution of the first several moments of $f^{(0)}$, standard equations emerge: the continuity equation, the ideal Euler equations, and the pressure (internal energy) equation. Under fairly mild assumptions, one also finds the associated pressure tensor is given by $P_{ij} = p\delta_{ij} - \mu(\nabla_i u_j + \nabla_j u_i) + \frac{2}{3}\mu\nabla \cdot \mathbf{u}\delta_{ij}$. Thus, one sees that in the collisional fluid case, $\Pi_{ij} = -2\mu D_{ij}$.

## 5. Channels of Transfer and Conversion in a Complex Cascade

Having formally described the channels of conversion made available in a two- (or multi-) species Vlasov plasma, we are now in a position to describe a complex plasma cascade in more detail.

At scales much larger than all kinetic scales, in plasmas such as the solar wind, the description of the cascade is vastly simplified. Kinetic effects in Ohm's law are negligible, and therefore, ion and electron densities and velocities are almost equal. For weak collisions, the resistivity is negligible, so the electric field at large scales and low frequencies is well approximated as $\mathbf{E} = -\mathbf{u} \times \mathbf{B} + \mathbf{D}$, where $\mathbf{D}$ is a weak nonideal dissipative contribution and $\mathbf{u}$ is the proton velocity. It is also reasonable to expect that the pressure averaged over large scales is isotropic. In such circumstances, the dynamics at the large, energy-containing scales is that of compressible MHD, which may be obtained approximately by computing moments of the Vlasov equation.

Whether the dynamics is incompressible (Hossain et al. 1995), nearly incompressible (Matthaeus & Brown 1988; Zank & Matthaeus 1991), or highly compressive (Mac Low 1999), one expects that the turbulent decay of the large-scale "energy-containing" eddies will follow a von Karman–Howarth description (de Kármán & Howarth 1938) appropriately generalized (Hossain et al. 1995; Biskamp 2003; Wan et al. 2012; Bandyopadhyay et al. 2018a) to MHD. However, as timescales become as small as the proton gyroperiod, and the length scales of interest approach the larger of the ion inertial scale and the thermal proton gyroradius, the fluid models break down, and the fluid description must be expanded to include kinetic effects.

Scale transfer in the plasma cascade is driven by advective nonlinearities such as $\mathbf{u}_\alpha \cdot \nabla \mathbf{u}_\alpha$ for species $\alpha$, in analogy to MHD scale transfer. Such cascades involve both the incompressible and compressible degrees of freedom (Yang et al. 2016). A significant feature here, distinct from a collisional fluid, is that there is a separate velocity cascade for each species labeled by $\alpha$. (Here, $\alpha$ will represent either ions $\alpha = i$ or electrons $\alpha = e$.) The cascades, especially the incompressible parts, are widely viewed as approximately local in scale, in the spirit of Kolmogorov theory (Kolmogorov 1941b).

Beyond advective cascade, other channels are available that lead to scale transfer as well as eventual dissipation. These channels—the work done on particles by the electromagnetic field and the conversion between flow energy and internal energy—couple the electromagnetic field to the first moment, i.e., the flow velocities, and the gradients of the first moment to the internal energy, that is, the sum of second central moments, of the velocity distributions. Other effects, not discussed here, contribute to anisotropies (Del Sarto et al. 2016) and higher-order moments of the particle vdf's. Eventually, the real space cascade gives rise to a velocity space cascade (Schekochihin et al. 2016; Servidio et al. 2017; Cerri et al. 2018; Pezzi et al. 2018), which then terminates through collisions and entropy production; these effects, however, require a model more complete than the Vlasov–Maxwell one (e.g., a Boltzmann model; Pezzi et al. 2016, 2019a; Pezzi 2017; Vafin et al. 2019).

A point of immediate emphasis is that all of the main channels of interest—the advective-driven scale transfer exemplified by the "LET," i.e., $\epsilon_r(\mathbf{x})$ in the third-order laws, as well as the electromagnetic work $\mathbf{J}_\alpha \cdot \mathbf{E}$, and the pressure–strain interaction
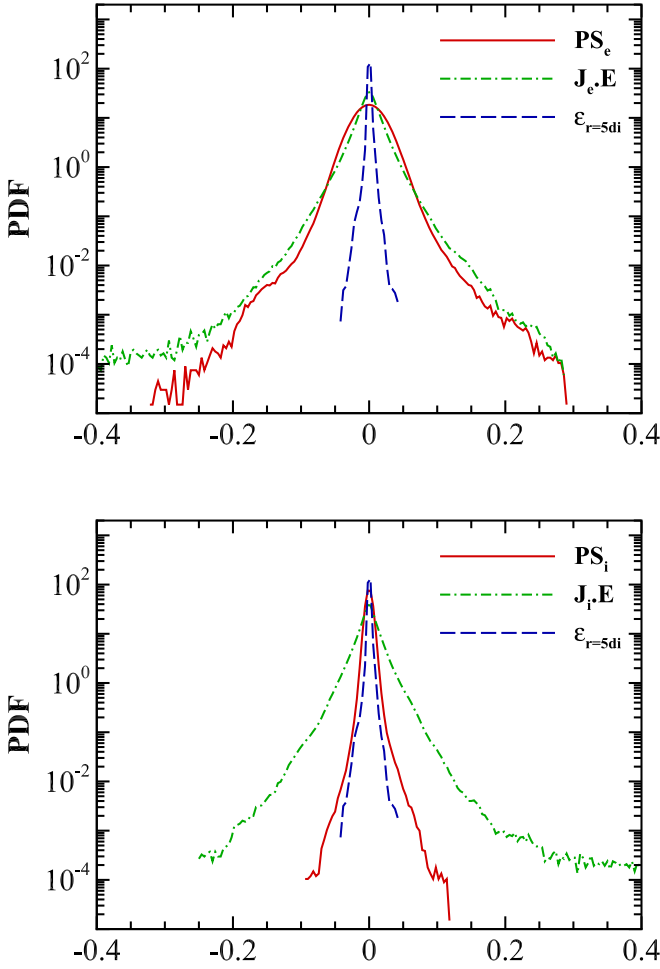
---

[9] The electromagnetic work done on charged particles in the electron fluid frame (sometimes with an additional small space charge correction) is called the Zenitani dissipation measure (Zenitani et al. 2011) and is widely used in reconnection studies. This quantity is also useful in turbulence analysis (Wan et al. 2012). It is also sometimes indicated simply as "the dissipation," a designation that we do not favor in view of the present detailed discussion.

**Figure 4.** PDFs of pressure–strain interaction ($PS_\alpha$), electromagnetic work done on particles ($\boldsymbol{J}_\alpha \cdot \boldsymbol{E}$), and LET $\epsilon_r$ measured at $r = 5d_i$, from a kinetic PIC simulation. (For details of the simulation, see Appendix A.) (Top): PDFs of $PS_\alpha$ and $\boldsymbol{J}_\alpha \cdot \boldsymbol{E}$ for electrons, and PDF of $\epsilon_{r=5d_i}$;. (Bottom): PDFs of $PS_\alpha$ and $\boldsymbol{J}_\alpha \cdot \boldsymbol{E}$ for protons, and PDF of $\epsilon_{r=5d_i}$. Note that in all cases, the PDF of $\epsilon_{r=5d_i}$ is narrowest. For electrons, the fluctuations (measured by breadth of the distribution) have more non-Gaussian tails for $\boldsymbol{J}_e \cdot \boldsymbol{E}$ and are more Gaussian for $PS_e$ but with similar width. For protons, the widths are largest for $\boldsymbol{J}_i \cdot \boldsymbol{E}$, and the $PS_i$ distribution is much narrower.

$PS_\alpha = -p_\alpha \theta_\alpha + PiD_\alpha$ for the species $\alpha$—have pointwise values of indefinite sign. As a consequence, the pointwise distributions of these quantities are broad, with the average values corresponding to a slight offset. This property is illustrated in Figure 4. Note that the broad sign-indefinite distributions of electromagnetic work and pressure–strain interaction are in this way analogous to the two-signed, broad distribution of the LET that underlies the third-order laws at inertial range (Sorriso-Valvo et al. 2018a, 2018b.

To build a picture of the plasma cascade, it is important to understand how the different transfer and conversion terms operate at varying spatial scales. To facilitate the analysis of energy conversion and scale transfer, we introduce a filtering operation that acts as a low-pass filter at scale $\ell$. See Appendix B for details. An overbar denotes a filtered quantity and a tilde denotes a density-weighted (Favre) filtered quantity. For example, the spatially filtered Vlasov equation is

$$\partial_t \bar{f}_\alpha + \boldsymbol{v} \cdot \nabla \bar{f}_\alpha + \frac{q_\alpha}{m_\alpha} \nabla_v \cdot \left( \overline{\boldsymbol{E} f_\alpha} + \frac{\boldsymbol{v}}{c} \times \overline{\boldsymbol{B} f_\alpha} \right) = 0. \quad (16)$$

To proceed with the analysis, we first define the relevant energies, the filtered fluid kinetic energy,

$$\widetilde{E}_\alpha^f = \frac{1}{2} \bar{\rho}_\alpha |\tilde{\boldsymbol{u}}_\alpha|^2, \quad (17)$$

and the filtered electromagnetic energy,

$$\overline{E}^m = \frac{1}{8\pi} (|\overline{\boldsymbol{B}}|^2 + |\overline{\boldsymbol{E}}|^2). \quad (18)$$

To obtain the time evolution of these energies (see Appendix B), we compute filtered moment equations using Equation (31), and after straightforward manipulations, obtain the required time derivatives. For the filtered fluid kinetic energy, we find

$$\partial_t \widetilde{E}_\alpha^f + \nabla \cdot \boldsymbol{J}_\alpha^u = -\boldsymbol{\Pi}_\alpha^{uu} - \boldsymbol{\Phi}_\alpha^{uT} - \boldsymbol{\Lambda}_\alpha^{ub}, \quad (19)$$

where we introduce the abbreviations

$$\boldsymbol{J}_\alpha^u = \widetilde{E}_\alpha^f \tilde{\boldsymbol{u}}_\alpha + \bar{\rho}_\alpha \tilde{\boldsymbol{\tau}}_\alpha^u \cdot \tilde{\boldsymbol{u}}_\alpha + \overline{\boldsymbol{P}}_\alpha \cdot \tilde{\boldsymbol{u}}_\alpha \quad (20)$$

for the spatial transport;

$$\boldsymbol{\Pi}_\alpha^{uu} = -(\bar{\rho}_\alpha \tilde{\boldsymbol{\tau}}_\alpha^u \cdot \nabla) \cdot \tilde{\boldsymbol{u}}_\alpha - q_\alpha / c\bar{n}_\alpha \tilde{\boldsymbol{\tau}}_\alpha^b \cdot \tilde{\boldsymbol{u}}_\alpha \quad (21)$$

for the flux of large-scale fluid flow energy transferred to subscale fluid flow energy;

$$\boldsymbol{\Phi}_\alpha^{uT} = -(\overline{\boldsymbol{P}}_\alpha \cdot \nabla) \cdot \tilde{\boldsymbol{u}}_\alpha \quad (22)$$

for the filtered pressure–strain interaction—the rate of conversion of fluid flow energy into internal energy; and

$$\boldsymbol{\Lambda}_\alpha^{ub} = -q_\alpha \bar{n}_\alpha \widetilde{\boldsymbol{E}} \cdot \tilde{\boldsymbol{u}}_\alpha \quad (23)$$

for the filtered $-\boldsymbol{J}_\alpha \cdot \boldsymbol{E}$—the rate of conversion of fluid flow energy into electromagnetic energy.

Similarly, the time evolution of the filtered electromagnetic energy is

$$\partial_t \overline{E}^m + \nabla \cdot \boldsymbol{J}^b = \sum_\alpha \boldsymbol{\Lambda}_\alpha^{ub} - \sum_\alpha \boldsymbol{\Pi}_\alpha^{bb}, \quad (24)$$

where

$$\boldsymbol{J}^b = \frac{c}{4\pi} (\overline{\boldsymbol{E}} \times \overline{\boldsymbol{B}}) \quad (25)$$

is the spatial transport;

$$\boldsymbol{\Lambda}_\alpha^{ub} = -q_\alpha \bar{n}_\alpha \widetilde{\boldsymbol{E}} \cdot \tilde{\boldsymbol{u}}_\alpha \quad (26)$$

is the rate of fluid flow energy conversion into electromagnetic energy; and

$$\boldsymbol{\Pi}_\alpha^{bb} = -q_\alpha \bar{n}_\alpha \tilde{\boldsymbol{\tau}}_\alpha^e \cdot \tilde{\boldsymbol{u}}_\alpha, \quad (27)$$

is the flux of electromagnetic energy across scales due to subscale work done by the electric field, where $\tilde{\boldsymbol{\tau}}_\alpha^e = (\widetilde{\boldsymbol{E}} - \overline{\boldsymbol{E}})$. Summing Equations (19) and (24), the filtered equation for the total fluid flow and electromagnetic energy takes the form

$$\partial_t \left( \sum_\alpha \widetilde{E}_\alpha^f + \overline{E}^m \right) + \nabla \cdot \left( \sum_\alpha \boldsymbol{J}_\alpha^u + \boldsymbol{J}^b \right)$$
$$= -\sum_\alpha \boldsymbol{\Pi}_\alpha^{uu} - \sum_\alpha \boldsymbol{\Pi}_\alpha^{bb} - \sum_\alpha \boldsymbol{\Phi}_\alpha^{uT}. \quad (28)$$

To illustrate the filtered transfer terms, we employ again a time snapshot from the kinetic PIC simulation described in Appendix A. As a first exercise, we focus on the scale-filtered
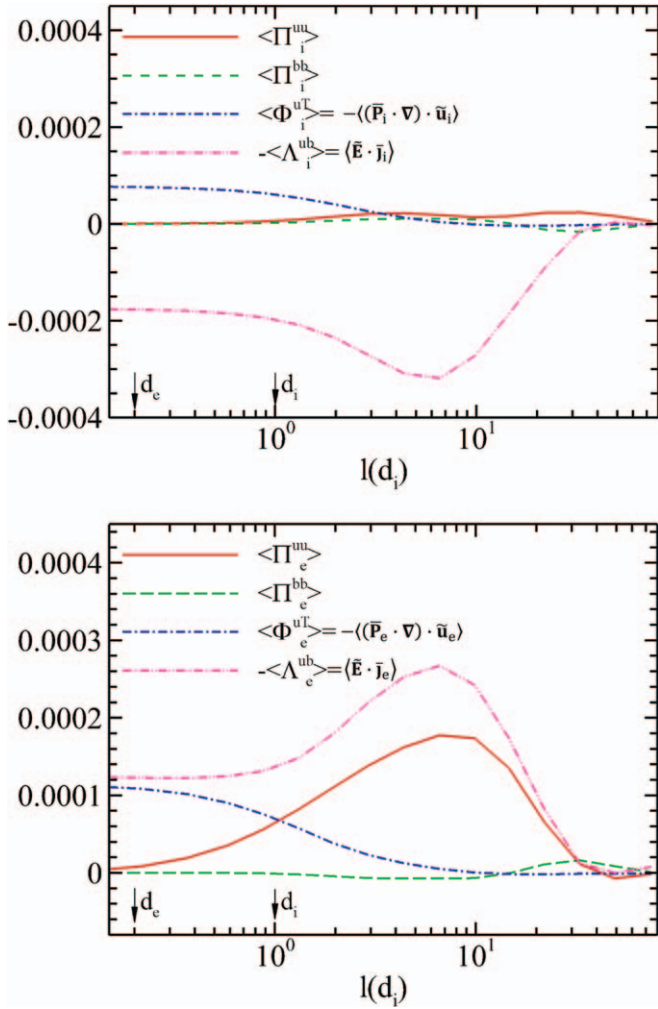
**Figure 5.** Volume-integrated scale-filtered energy transfer terms: scale-to-scale fluxes $\langle \Pi_\alpha^{uu} \rangle$ and $\langle \Pi_\alpha^{bb} \rangle$, filtered electromagnetic work on particles $\langle \tilde{E} \cdot \bar{J}_\alpha \rangle$, and filtered pressure–strain interaction $\langle -(\bar{P}_\alpha \cdot \nabla) \cdot \tilde{u}_\alpha \rangle$, for species $\alpha$ from a kinetic PIC simulation (see the Appendix). (Top) Filtered energy transfer terms vs. filtering scales for ions. (Bottom) Filtered energy transfer terms vs. filtering scales for electrons.



**Figure 6.** Cascade effects summed over species. Volume-integrated scale-to-scale flux $\langle \sum_\alpha \Pi_\alpha^{uu} + \sum_\alpha \Pi_\alpha^{bb} \rangle$, filtered pressure–strain interaction $\langle \sum_\alpha \Phi_\alpha^{uT} \rangle = -\langle \sum_\alpha (\bar{P}_\alpha \cdot \nabla) \cdot \tilde{u}_\alpha \rangle$, and estimate of transfer rate from third-order moment. The horizontal reference line at ∼0.0002 suggests the approximate level of the inertial range flux. See discussion in the text.

convective transfer, pressure–strain, and electromagnetic work separately for each species, and as a function of scale. These quantities are illustrated in Figure 5. For protons, we see that the convective transfer induces negative electromagnetic work that builds up magnetic energy throughout an inertial range. At smaller scales approaching $d_i$, the pressure strain is converting flow energy into internal energy of protons. In the lower panel of Figure 5, the same filtered quantities are shown for the electrons. The picture is quite different, owing to the difference in proton and electron intrinsic inertia (mass). Here, the electrons see the strong onset of electromagnetic energy conversion into electron flow, giving rise to an inertial range signified by peaks over a range of scales of both quantities. Like the protons, the electron contribution to convective transfer and electromagnetic work diminishes in intensity approaching kinetic scales near $d_i$. Over a similar range, approaching $d_i$ from above and extending to the electron inertial scale $d_e$, the pressure–strain interaction becomes progressively more important.

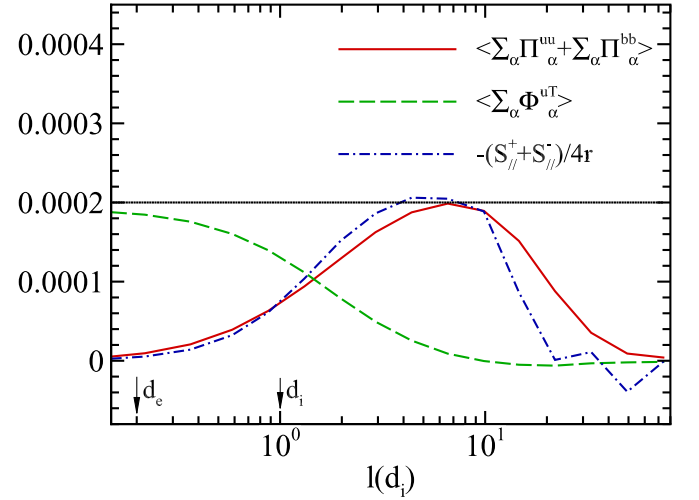A view of the net effect of the transfer associated with both species is shown in Figure 6. Illustrated are the relevant cascade terms summed over species: the scale-to-scale flux due to advection, the scale-filtered pressure–strain interaction, and the total (sum over the two Elsässer variables) of the third-order energy transfer. Here we see the intuitive result that the third-order law closely follows the scale-to-scale flux, each delineating an expected (even if narrow) inertial range. The level of inertial range transfer is suggested by the horizontal reference line at ∼0.0002. As the inertial range transfer diminishes approaching $d_i$, the total filtered pressure–strain effect increases toward smaller scales, approaching the same reference line at subelectron scales. This clearly indicates that the kinetic range is associated with a suppression of the standard cascade terms in favor of the production of internal energy.

A diagrammatic representation of the pathways to dissipation is described in Figure 7. Overall, the transfer from scale to scale is believed, with substantial and growing empirical support, to proceed in a way that is analogous to the Kolmogorov cascade. The transfer is necessarily more complex in a collisionless multispecies plasma.

## 6. Kinetic Activity and Coherent Spatial Structures

Coherent structures in the magnetic and plasma flow (Dmitruk et al. 2004; Markovskii et al. 2006; Parashar et al. 2011; Dalena et al. 2014; Drake et al. 2014; Wan et al. 2015) play an important role in heating, as is confirmed in observations (Retinò et al. 2007; Osman et al. 2011). These structures typically have one or more dimensions on the order of an ion inertial scale (Dmitruk & Matthaeus 2006; Markovskii & Vasquez 2011; Wang et al. 2013; Makwana et al. 2015). The dynamical processes that occur in association with these structures include energization by direct (parallel) electric fields, strong scattering and confinement leading to stochastic orbits, betatron effect, and pickup by flows through the $E \times B$ drift effect. These effects have been parameterized in various phenomenologies (Ambrosiano et al. 1988; Drake et al. 2006; Chandran et al. 2010; Shay et al. 2014; le Roux et al. 2015). The net effect of these processes, and notably their localization in structured patterns reflecting the magnetic structure of the turbulence, is evident in simulations. Hybrid Vlasov simulations
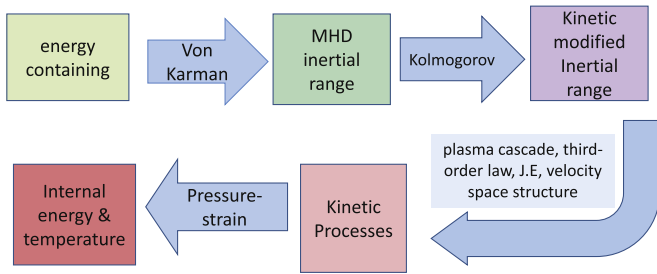
**Figure 7.** Collapsing the complex pathways into four transfer rates. Complex pathways and channels lead to dissipation in weakly collisional plasma. Each species engages in scale-to-scale transfer, analogous to a Kolmogorov cascade. Each species also exchanges energy with the electromagnetic field. The pressure–strain interactions, both pressure dilatation and PiD types, exchange energy between the flow of each species and the corresponding internal energy of that species.

have permitted these associations for protons to be studied in some detail (Greco et al. 2012; Servidio et al. 2012, 2014, 2015).

Based on prior results showing the formation of coherent structures in MHD and plasma, it should not be at all surprising to find that the physical quantities that are responsible for the transfer and conversion of energy in collisionless plasmas are also found in the same kinds of spatial concentrations. Figure 8 illustrates the formation of several types of coherent spatial structures in a well-resolved kinetic PIC simulation (see Appendix A).

The top panels show the electric current density and the LET at a scale of $5d_i$, exhibiting the type of spatial concentration familiar even in MHD simulations. The next row shows maps of the electromagnetic work $J_\alpha \cdot E$ on electrons and protons. Below that is illustrated the pressure–strain interaction for electrons and protons, respectively. The following row shows the scale-to-scale transfer for electrons and protons. Finally, the last row shows the spatial distribution of electron temperature and proton temperature.

The electrons are hottest near sites of the strongest thin current sheets. Proton hot spots are relatively broader and are concentrated around the strong currents near magnetic "islands," and the interaction region between pairs of islands (Ambrosiano et al. 1988; Dmitruk et al. 2004; Chandran et al. 2010; Shay et al. 2014). The spatial coincidence of all of the above quantities is of the type that may be called regional correlation (Yang et al. 2019), meaning that the quantities may be found in nearby regions or even interleaved with one another, so that pointwise correlations can be small, but coarse-grained correlations substantial.

## 7. Dissipation, Entropy, and a Thought Experiment

Any discussion of turbulent cascade in collisionless Vlasov plasma leads inevitably to the question of what one means by "dissipation." Here we have adopted the definition, perhaps not universally agreed upon, that energy is dissipated when the dynamics leads to the global reduction of total energy in the electromagnetic field and in the fluid velocity fluctuations in all species, while internal energy summed over species, increases. While variations of this meaning may be encountered, this definition has the advantage in the sense that the transfer of energy due to cascade leads to its reduction by "dissipative processes," in direct analogy to the viscous-collisional case.

Within the context of this definition, there are important questions about dissipation that arise. For example, the pathways leading to dissipation, as we have discussed above, emerge from the Vlasov equation. Critics may note that the Boltzmann entropy $S = -k \int d^3x \int d^3v \, f \ln f$ is invariant in time for Vlasov–Maxwell dynamics. Then, if one assumes that there is always a one-to-one relation between this definition of entropy and the temperature, one might conclude that dissipation (and associated heating) cannot occur in a Vlasov formalism. Or, if it does, it must be due to numerical artifacts. A similar and also familiar criticism of a Vlasov-based theory of dissipation is the argument that the Vlasov equation is reversible due to the lack of collisions, and therefore it cannot describe dissipation, which is claimed to be inherently irreversible.

Our perspective is that neither of the above arguments is completely accurate. Regarding the argument based on invariance of entropy in a Vlasov theory, we note that the entropy defined above as $S$ is the Boltzmann entropy, and this is distinct from the Clausius (or "thermodynamic") entropy. It is not obvious that the Boltzmann entropy so defined is the correct entropy to describe the statistical dynamics of turbulent Vlasov dissipation. In particular, the Clausius entropy, with its connection to temperature, is well defined only in LTE, while the Boltzmann entropy does not take into account explicit contributions from turbulence (Goldstein & Lebowitz 2004). There are an infinite number of invariants of the Vlasov equation (e.g., any function $Q(f)$); one of these is the Boltzmann entropy, but we are unaware whether it has been demonstrated that this functional is a fully useful definition of entropy in a strongly turbulent Vlasov plasma.

Regarding the second argument, and reversibility, we note that classical mechanics is always formally reversible. Therefore, not only Vlasov, but also $N$-body classical dynamics, is reversible, even when collisions are included. While classical collisions are reversible, it is the approximations inherent in collision operators that introduce formal irreversibility. Of course, in a reversible system with a large number of degrees of freedom (Ford 1992), the recurrence time becomes astronomically large, except for very special initial conditions.[10]

It should be clear from considerations such as those above that the Boltzmann entropy $S = -k \int d^3x \int d^3v \, f \ln f$ is of limited utility in a turbulent collisionless plasma. The two main reasons for this—lack of collisions and the lack of complete treatment of turbulence (Goldstein & Lebowitz 2004)—are often discussed, usually without clear conclusions. There has been recent interest in studying the conservation of $S$ in the absence of collisions (Liang et al. 2019); such studies lead to clarification of the spatial distribution of entropy and provide useful tests of the resolution of collisionless PIC kinetic codes. Other recent studies examine the systematic effects of including collisions in a kinetic model (Daughton et al. 2009), notably including changes of entropy $S$ (Liang et al. 2019; Pezzi et al. 2019a). This active area of research is providing insights into issues such as the relationship of entropy to velocity space structure (Pezzi et al. 2019b), the spatial distribution of dissipation (Howes et al. 2011), and the effect of collisions on the rate of magnetic reconnection (Daughton et al. 2011b).

---

[10] It is important to keep in mind that the Vlasov description is an approximation, specifically a mean field theory, in which properties of individual particles, including their coordinates, do not appear explicitly, while the associated interparticle forces, are treated as negligible and ignored.
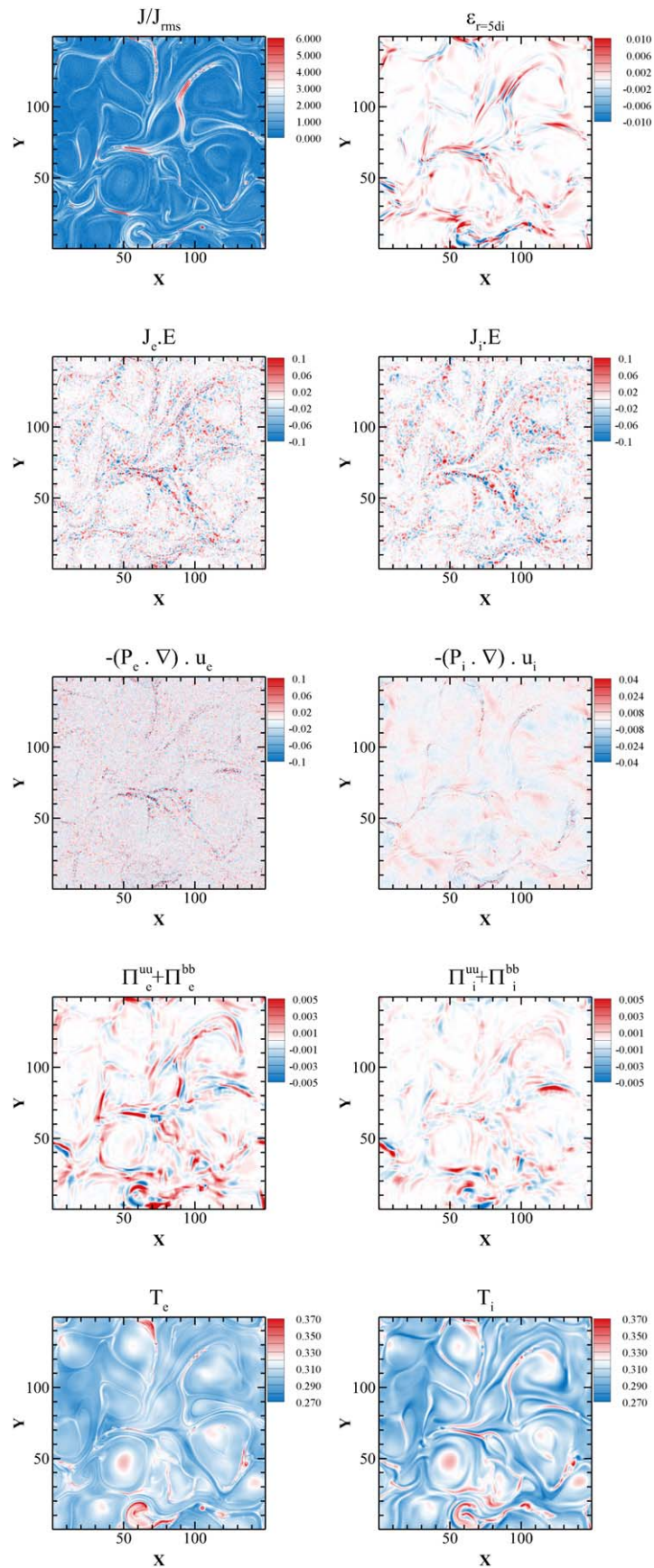
**Figure 8.** Contour maps of normalized electric current density $J/J_{\rm rms}$, LET $\epsilon_{r=5d_i}$, electromagnetic work $\boldsymbol{J}_\alpha \cdot \boldsymbol{E}$ on electrons and ions, pressure–strain interaction $PS_\alpha$ for electrons and ions, scale-to-scale flux $\Pi_\alpha^{uu} + \Pi_\alpha^{bb}$ for electrons and ions, and electron and ion temperature $T_\alpha$. It is apparent that all quantities have elevated activity in similar small subregions, suggesting intermittency. However, examined in greater detail (not shown), there are no strong pointwise correlations among these quantities.

Some of the subtle aspects of the relationship between fluid and thermodynamic entropies, especially with regard to anisotropic and nongyrotropic fluids, have been discussed in an interesting recent paper by Du et al. (2019).

As a mean field theory that ignores particle correlations, the Vlasov system is manifestly incomplete, but nevertheless important physics may be addressed within this limited context. In particular, because the Vlasov–Maxwell system is frequently employed to study plasma turbulence, it is reasonable to ask— what is the nature of entropy, and dissipation, in these solutions? In spite of the large amount of recent studies on the subject, one may observe from the discussion and frequent disagreement at conferences that there is a lack of consensus on these issues, and even on the definition of dissipation itself.

To organize thoughts on the subject, we propose here a gedanken experiment that we suggest may clarify some of these issues. The experiment itself is numerical, and while it would be very illuminating to actually perform such a simulation, it is our opinion that its implementation would be intractably difficult at present. We will, however, propose a hypothesis concerning its results.

Let us consider a large ($L/d_i \gg 1$) electron–proton plasma in a periodic (isolated) domain. For simplicity, assume the electrons are collisionless and that there are no electron–proton collisions. Now consider the evolution of this plasma in two distinct cases: collisionless protons and weakly collisional protons.

We make the following assertions:

1. The collision operator conserves momentum and energy. Therefore, collisions alone cannot change energy from flows into the trace of the pressure tensor, i.e., into the reservoir of internal energy. The above property means that collisions do not contribute directly to "heating," for example, in a uniform homogeneous flow at finite "temperature."
2. Whether or not there are collisions, the pressure–strain interactions, $p\theta$ and $PiD$, can convert energy between flows and the second central moment of distribution functions.
3. Collisions act to limit the distortions of the ion vdf's, i.e., the local effect of collisions is to smooth the vdf's.
4. When there are no collisions, the Boltzmann entropy $S = -k\langle f \ln f \rangle_{x,v}$ (B-entropy) is a constant. This Boltzmann entropy coincides with the thermodynamic entropy (Clausius, or C-entropy) only when the system is in thermal equilibrium.

With these ideas in mind, we formulate an illustrative thought experiment as follows (see Figure 9):

1. A simulation is initiated with incompressible turbulent fluctuations at large scales. There are no collisions. A cascade develops in time.
2. The cascade causes degeneration or "dissipation" of large-scale fluctuation in velocities and electromagnetic fields. The Boltzmann entropy stays constant during the process, while energy is exchanged, finding its way into internal energy. The increase of the second central moment, i.e., the kinetic temperature, while B-entropy remains constant is very different from the state of affairs in collisional gas dynamics that remains always in LTE.
3. After many eddy turnover (large-scale nonlinear) times have transpired, almost all the energy has disappeared from
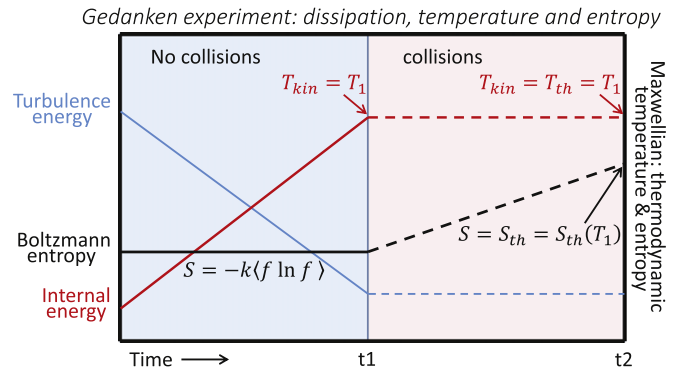


*Gedanken experiment: dissipation, temperature and entropy*

**Figure 9.** Diagram of a thought experiment discussed in the text, intended to clarify the relationships among Vlasov dissipation, temperature, collisions, and entropy. An idealized proton–electron kinetic (Vlasov) code is initialized with a large (many $d_i$) sample of nearly incompressible fluctuations. The turbulent evolution causes the decay of fluctuation energy until time $t1$, during which time the Boltzmann entropy $S$ remains constant while the proton internal energy increases. At time $t1$, almost all fluctuation energy is dissipated and the proton kinetic temperature has increased to a value $T_{kin}$. Now, proton–proton collisions are "turned on." Subsequently, the Boltzmann entropy increases, and the kinetic temperature of protons remains essentially constant. At some later time $t2$, the protons are at or close to Maxwellian distributions. We expect that the thermodynamic temperature $T_{th}$ and kinetic temperature $T_{kin}$ will now be equal and the thermodynamic entropy $S_{th}$ will equal the Boltzmann entropy $S = S(T_{th})$ at thermodynamic temperature $T_{th}$.

macroscopic, fluid-scale fluctuations. Because energy is conserved, it is clear that energy has been transferred into kinetic-scale degrees of freedom, and we assume that most of this energy resides the particle's kinetic energy. The associated temperature increase has slowed drastically, and the kinetic temperature is almost constant, near a value $T1$ (See Figure 9). But with little or no energy left to dissipate, the temperature cannot increase appreciably after this time. We may therefore, to a reasonable approximation, compute the equivalent C-entropy based on $T1$. We write down this number as a prediction, even though Clausius is not applicable to this state, which is not in an LTE/Maxwellian state.

4. At this point, time $t1$, the collisions are turned on and the system continues to evolve. The Boltzmann entropy increases during this period. However, the kinetic temperature cannot increase because total energy is conserved, and the supply of fluctuation energy was exhausted prior to time $t1$.

5. The collisions cause the evolution after time $t1$ to approach a local Maxwellian (or even a global Maxwellian). When a Maxwellian state is achieved to a good approximation, the simulation is stopped at time $t2$.

6. Now compute the B-entropy and the C-entropy. They will agree. They will also agree with the equivalent C-entropy we wrote down in step 3. Therefore, this experiment enables a "prediction" of the final Boltzmann entropy using a Vlasov simulation (having no collisions.)

We offer this as a hypothesis regarding the outcome of the thought experiment. If this hypothesis were to be verified, we suggest that this sequence of events would serve to clarify the roles of entropy/collisions and temperature/pressure–strain in dissipation.

We have seen that in order to heat the plasma, one needs the pressure tensor to interact with flow gradients. Collisions indirectly contribute to heating, e.g., scattering particles and subsequently changing the off-diagonal pressure tensor in nearby locations. Note that turbulence, e.g., through pitch angle scattering, does that as well, so the role of collisions in this

regard is not unique. The conclusion is that, under the assumed circumstances, collisions act to increase the B-entropy, but collisions cannot change the temperature. In this sense, temperature and entropy are, in general, independent concepts, even though they coincide completely only in thermal equilibrium.

## 8. Discussion: Recovering a Complex Cascade in Vlasov–Maxwell Plasma

We have reviewed current understanding of the pathways to energy dissipation in a proton–electron Vlasov–Maxwell plasma, focusing mainly on the available channels for energy conversion. Most of our discussion extends readily from the simplest incompressible MHD model to more complex multi-component collisionless plasma models.

The interaction between the pressure tensors and the gradients of the velocity fields (for each species) occupies a particularly important role, as these couplings are responsible for exchanges between flows and internal energies. The pressure–gradient couplings are conveniently decomposed into pressure–dilatation and pressure–strain interactions. These interactions are not single-signed and are observed to be broadly distributed, with a relatively small net value (compared to their half-widths) corresponding to the increase of internal energy. In this regard, pressure–strain interaction is similar to electromagnetic work on particles and to the unaveraged Kolmogorov–Yaglom third-order correlations (Kolmogorov 1941a; Politano & Pouquet 1998), which also are not single-signed, have broad distributions, and usually have small net values after suitable averaging. All of these quantities also admit highly nonuniform distributions in space, corresponding to different facets of intermittency.

An interesting feature, revealed by scale filtering, is that there are different ranges of scales in which each type of transfer and conversion is most effective, or even dominant over the others. In addition, other papers have shown that transfer into compressive modes occurs mainly at larger scales (Aluie 2011; Aluie et al. 2012). In the inertial range, the Kolmogorov incompressible transfer occurs without loss over the extent of the power-law range, while the compressive cascade operates almost in parallel. Approaching kinetic scales, the non-MHD part of the electromagnetic work on protons and electrons becomes significant, with work on protons occurring at somewhat larger scales. The key step of pressure–strain conversion turns on strongly at subproton scales, leading to robust production of internal energy at subproton kinetic scales.

The large fluctuations observed in the main channels of transfer and conversion, the LET, the electromagnetic work ($J \cdot E$), and the pressure–strain interactions ($p\theta$ and PiD) are an intrinsic feature of plasma turbulence. The relatively small average values of these quantities support the cascade itself, transferring toward smaller scales and through small-scale fluid velocity gradients, into internal energy.

Our current perspective is that, in this collisionless system, the disappearance of macroscopic flow and magnetic field fluctuations, and increase of internal energy are driven solely by the enormous numbers of degrees of freedom available at the level of thermal motions relative to those available to fluid motions. Based on this idea, which we regard as plausible but unproven, we developed the thought experiment described in Section 7, which we offer as a hypothesis to clarify the role of B-entropy and temperature in this type of collisionless dissipation.

The above ideas concerning dissipation of turbulence in the Vlasov–Maxwell regime are consistent with current knowledge, largely based on inferences derived from numerical experiments, and observations. Clearly, these cannot be viewed as proven or rigorous in any sense. The closest theoretical analogy that we envision as supporting this perspective is our current understanding of the Gibbsian absolute equilibrium ensemble treatment of an ideal Galerkin truncated incompressible fluid and MHD turbulence (Frisch et al. 1975; Kraichnan & Montgomery 1980; Stribling & Matthaeus 1990; Shebalin 1996). In those cases, the dynamics are fully ideal, with dissipation coefficients such as viscosity and resistivity absent. However, numerous computer experiments have shown that these systems essentially always relax to a predictable statistical state that maximizes a suitably defined entropy. This description qualitatively aligns with the present treatment of Vlasov–Maxwell turbulence, but also hints at several caveats. An important limitation is that in the Gibbsian case, the correct entropy is apparently known, and it involves all available degrees of freedom. Meanwhile, in the plasma case, we can only suggest at present that a generalization of the Boltzmann entropy might be developed that includes the turbulent fluctuations properly and would then describe the dissipation process itself. Second, in the Gibbsian fluid case, it is well known that the approach to the statistical state sometimes involves strong transfer to the largest scale, a phenomenon known as (Bose) condensation (Kraichnan & Montgomery 1980; Servidio et al. 2008a). By analogy, in the plasma case, dynamics associated with dynamo action might also cause a reversal of scale transfer and of electromagnetic work, so that the overall diagrammatic description of the cascade would need to be appropriately modified. We therefore must conclude with the caveat that the plasma turbulence cascade is not likely to be universal in any meaningful sense. Consequently, the conclusions and hypotheses we offer here, based mainly on the analysis of weakly compressible, solar wind-like plasma conditions (near equipartition, plasma beta order unity, etc.), may require modifications when plasma parameters vary into other regimes.

## Appendix A
## Simulation

The kinetic simulation used in this paper was performed using the fully electromagnetic particle-in-cell code P3D (Zeiler et al. 2002) in 2.5D (three components of dependent field vectors and a two-dimensional spatial grid) geometry. The simulation was performed in a periodic domain, whose size is $L = 149.5648d_i$, with $4096^2$ grid points and 3200 particles of each species per cell ($\sim 107 \times 10^9$ total particles). The ion to electron mass ratio is $m_i/m_e = 25$, and the speed of light in the simulation is $c = 15v_{Ar}$ ($v_{Ar}$ is the Alfvén speed). The run is a decaying initial value problem, starting with uniform density ($n_0 = 1.0$) and temperature of ions and electrons ($T_0 = 0.3$). The uniform magnetic field is $B_0 = 1.0$ directed out of the plane. We analyzed statistics using a snapshot near

the time of maximum root mean square (rms) electric current density. Prior to statistical analyses, we removed noise inherent in the particle-in-cell plasma algorithm through low-pass Fourier filtering of the fields. This simulation was also used to study kinetic plasma turbulence as a function of plasma $\beta$ (Parashar et al. 2018) and scale dependence of energy transfer in turbulent plasma (Yang et al. 2019).

## Appendix B
## Filtering

This Appendix briefly describes the filtering technique employed in Section 5 of the paper. The spatially filtered $f_\alpha$ in Equation (15) is given by

$$\bar{f}_\alpha(\boldsymbol{x}, \boldsymbol{v}, t) = \int f_\alpha(\boldsymbol{x}', \boldsymbol{v}, t) G_l(\boldsymbol{x} - \boldsymbol{x}') d\boldsymbol{x}', \quad (29)$$

where $G_\ell(\boldsymbol{r}) = \ell^{-3}G(\boldsymbol{r}/\ell)$ is a filtering kernel and $G(\boldsymbol{r})$ is a normalized boxcar window function. The low-pass filtered $\bar{f}_\alpha$ only contains information at length scales $>\ell$.

The filtering operation can commute with derivative operations, i.e.,

$$\overline{\partial_t f_\alpha} = \partial_t \bar{f}_\alpha, \quad \overline{\nabla f_\alpha} = \nabla \bar{f}_\alpha, \quad \overline{\nabla_v f_\alpha} = \nabla_v \bar{f}_\alpha. \quad (30)$$

Then, the spatially filtered Vlasov equation is written as

$$\partial_t \bar{f}_\alpha + \boldsymbol{v} \cdot \nabla \bar{f}_\alpha + \frac{q_\alpha}{m_\alpha} \nabla_v \cdot \left( \overline{\boldsymbol{E} f_\alpha} + \frac{\boldsymbol{v}}{c} \times \overline{\boldsymbol{B} f_\alpha} \right) = 0. \quad (31)$$

From Equation 31, moment equations for each species yields

$$\partial_t \bar{\rho}_\alpha + \nabla \cdot (\overline{\rho_\alpha \boldsymbol{u}_\alpha}) = 0, \quad (32)$$

$$\partial_t (\overline{\rho_\alpha \boldsymbol{u}_\alpha}) + \nabla \cdot (\overline{\rho_\alpha \boldsymbol{u}_\alpha \boldsymbol{u}_\alpha})$$
$$= -\nabla \cdot \overline{\boldsymbol{P}_\alpha} + q_\alpha (\overline{n_\alpha \boldsymbol{E}} + \overline{n_\alpha \boldsymbol{u}_\alpha/c \times \boldsymbol{B}}). \quad (33)$$

A Favre-filtered (density-weighted-filtered) field (Favre 1969) is defined as

$$\tilde{\boldsymbol{a}} = \overline{n\boldsymbol{a}}/\bar{n}. \quad (34)$$

Then, the moment equations aforementioned can be written as

$$\partial_t \bar{\rho}_\alpha + \nabla \cdot (\bar{\rho}_\alpha \tilde{\boldsymbol{u}}_\alpha) = 0, \quad (35)$$

$$\partial_t (\bar{\rho}_\alpha \tilde{\boldsymbol{u}}_\alpha) + \nabla \cdot (\bar{\rho}_\alpha \tilde{\boldsymbol{u}}_\alpha \tilde{\boldsymbol{u}}_\alpha) = -\nabla \cdot (\bar{\rho}_\alpha \tilde{\boldsymbol{\tau}}_\alpha^u)$$
$$+ q_\alpha/c \bar{n}_\alpha \tilde{\boldsymbol{\tau}}_\alpha^b - \nabla \cdot \overline{\boldsymbol{P}_\alpha} + q_\alpha \bar{n}_\alpha (\widetilde{\boldsymbol{E}} + \tilde{\boldsymbol{u}}_\alpha/c \times \widetilde{\boldsymbol{B}}), \quad (36)$$

where $\tilde{\boldsymbol{\tau}}_\alpha^u = (\widetilde{\boldsymbol{u}_\alpha \boldsymbol{u}_\alpha} - \tilde{\boldsymbol{u}}_\alpha \tilde{\boldsymbol{u}}_\alpha)$ and $\tilde{\boldsymbol{\tau}}_\alpha^b = (\widetilde{\boldsymbol{u}_\alpha \times \boldsymbol{B}} - \tilde{\boldsymbol{u}}_\alpha \times \widetilde{\boldsymbol{B}})$.

## ORCID iDs

William H. Matthaeus https://orcid.org/0000-0001-7224-6024
Yan Yang https://orcid.org/0000-0003-2965-7906
Tulasi N. Parashar https://orcid.org/0000-0003-0602-8381
Riddhi Bandyopadhyay https://orcid.org/0000-0002-6962-0959
Oreste Pezzi https://orcid.org/0000-0002-7638-1706
Francesco Valentini https://orcid.org/0000-0002-1296-1971

## References

Alexakis, A. 2007, ApJL, 667, L93
Alexakis, A., Bigot, B., Politano, H., & Galtier, S. 2007, PhRvE, 76, 056313
Aluie, H. 2011, PhRvL, 106, 174502
Aluie, H., Li, S., & Li, H. 2012, ApJL, 751, L29
Ambrosiano, J., Matthaeus, W. H., Goldstein, M. L., & Plante, D. 1988, JGR, 93, 14383
Andrés, N., Sahraoui, F., Galtier, S., & Hazid, L. Z. 2018, JPlPh, 84, 905840404
Bandyopadhyay, R., Chasapis, A., Chhiber, R., et al. 2018a, ApJ, 866, 106
Bandyopadhyay, R., Oughton, S., Wan, M., et al. 2018b, PhRvX, 8, 041052
Banerjee, N., & Sharma, P. 2014, MNRAS, 443, 687
Biskamp, D. 2003, Magnetohydrodynamic Turbulence (Cambridge: Cambridge Univ. Press)
Bruno, R., & Carbone, V. 2013, LRSP, 10, 2
Cerri, S., Kunz, M. W., & Califano, F. 2018, ApJL, 856, L13
Chandran, B. D. G., & Cowley, S. C. 1998, PhRvL, 80, 3077
Chandran, B. D. G., Li, B., Rogers, B. N., Quataert, E., & Germaschewski, K. 2010, ApJ, 720, 503
Chasapis, A., Yang, Y., Matthaeus, W. H., et al. 2018, ApJ, 862, 32
Coburn, J. T., Forman, M. A., Smith, C. W., Vasquez, B. J., & Stawarz, J. E. 2015, RSPTA, 373, 20140150
Cranmer, S. R. 2009, LRSP, 6, 3
Dalena, S., Rappazzo, A. F., Dmitruk, P., Greco, A., & Matthaeus, W. H. 2014, ApJ, 783, 143
Daughton, W., Roytershteyn, V., Albright, B. J., et al. 2009, PhPl, 16, 072117
Daughton, W., Roytershteyn, V., Karimabadi, H., et al. 2011a, NatPh, 7, 539
Daughton, W., Roytershteyn, V., Karimabadi, H., et al. 2011b, in AIP Conf. Ser. 1320, Modern Challenges in Nonlinear Plasma Physics, ed. D. Vassiliadis (New York: AIP), 144
de Kármán, T., & Howarth, L. 1938, RSPSA, 164, 192
Del Sarto, D., Pegoraro, F., & Califano, F. 2016, PhRvE, 93, 053203
Dmitruk, P., & Matthaeus, W. H. 2006, PhPl, 13, 2307
Dmitruk, P., Matthaeus, W. H., & Seenu, N. 2004, ApJ, 617, 667
Drake, J. F., Swisdak, M., Cassak, P. A., & Phan, T. D. 2014, GeoRL, 41, 3710
Drake, J. F., Swisdak, M., Che, H., & Shay, M. A. 2006, Natur, 443, 553
Du, S., Zank, G.P., Guo, F., & Li, X. 2019, arXiv:1911.08086
Eyink, G. L. 2005, PhyD, 207, 91
Favre, A. 1969, SIAM, 1969, 231
Ford, J. 1992, PhR, 213, 271
Frisch, U., Pouquet, A., Léorat, J., & Mazure, A. 1975, JFM, 68, 769
Goldstein, S., & Lebowitz, J. L. 2004, PhyD, 193, 53
Greco, A., Valentini, F., Servidio, S., & Matthaeus, W. H. 2012, PhRvE, 86, 066405
Hadid, L. Z., Sahraoui, F., Galtier, S., & Huang, S. 2018, PhRvL, 120, 055102
Hellinger, P., Verdini, A., Landi, S., Franci, L., & Matteini, L. 2018, ApJL, 857, L19
Hossain, M., Gray, P. C., Pontius, D. H., Jr., Matthaeus, W. H., & Oughton, S. 1995, PhFl, 7, 2886
Howes, G. G., Tenbarge, J. M., Dorland, W., et al. 2011, PhRvL, 107, 035004
Jokipii, J. R. 1966, ApJ, 146, 480
Karimabadi, H., Roytershteyn, V., Wan, M., et al. 2013, PhPl, 20, 012303
Klainerman, S., & Majda, A. 1981, CPAM, 34, 481
Kolmogorov, A. N. 1941a, C.R. Acad. Sci.U.R.S.S., 32, 16, [Reprinted in RSPSA 434, 15–17 (1991)]
Kolmogorov, A. N. 1941b, Dokl. Akad. Nauk SSSR, 30, 301, [Reprinted in RSPSA 434, 9–13 (1991)]
Kolmogorov, A. N. 1962, JFM, 13, 82
Kraichnan, R. H., & Montgomery, D. C. 1980, RPPh, 43, 547
Lazarian, A., Eyink, G. L., & Vishniac, E. T. 2012, PhPl, 19, 012105
le Roux, J. A., Zank, G. P., Webb, G. M., & Khabarova, O. 2015, ApJ, 801, 112
Liang, H., Cassak, P. A., Servidio, S., et al. 2019, PhPl, 26, 082903
Mac Low, M. 1999, ApJ, 524, 169
Makwana, K., Zhdankin, V., Li, H., Daughton, W., & Cattaneo, F. 2015, PhPl, 22, 042902
Mallet, A., Schekochihin, A. A., & Chandran, B. D. G. 2017, MNRAS, 468, 4862
Markovskii, S. A., & Vasquez, B. J. 2011, ApJ, 739, 22
Markovskii, S. A., Vasquez, B. J., Smith, C. W., & Hollweg, J. V. 2006, ApJ, 639, 1177
Matthaeus, W. H., & Brown, M. R. 1988, PhFl, 31, 3634
Matthaeus, W. H., & Lamkin, S. L. 1986, PhFl, 29, 2513
Matthaeus, W. H., & Velli, M. 2011, SSRv, 160, 145
Orszag, S. A. 1977, in Fluid Dynamics, ed. R. Balian & J.-L. Peube (New York: Gordon and Breach), 235
Osman, K. T., Matthaeus, W. H., Greco, A., & Servidio, S. 2011, ApJL, 727, L11
Parashar, T. N., Matthaeus, W. H., & Shay, M. A. 2018, ApJL, 864, L21
Parashar, T. N., Servidio, S., Shay, M. A., Breech, B., & Matthaeus, W. H. 2011, PhPl, 18, 092302

Pezzi, O. 2017, JPlPh, 83, 555830301
Pezzi, O., Perrone, D., Servidio, S., et al. 2019a, ApJ, 887, 208
Pezzi, O., Servidio, S., Perrone, D., et al. 2018, PhPl, 25, 060704
Pezzi, O., Valentini, F., & Veltri, P. 2016, PhRvL, 116, 145001
Pezzi, O., Yang, Y., Valentini, F., et al. 2019b, PhPl, 26, 072301
Politano, H., & Pouquet, A. 1998, GeoRL, 25, 273
Pope, S. B. 2000, Turbulent Flows (Cambridge: Cambridge Univ. Press)
Retinò, A., Sundkvist, D., Vaivads, A., et al. 2007, NatPh, 3, 236
Schekochihin, A. A., Parker, J. T., Highcock, E. G., et al. 2016, JPlPh, 82, 905820212
Servidio, S., Chasapis, A., Matthaeus, W. H., et al. 2017, PhRvL, 119, 205101
Servidio, S., Matthaeus, W. H., & Carbone, V. 2008a, PhPl, 15, 042314
Servidio, S., Matthaeus, W. H., & Dmitruk, P. 2008b, PhRvL, 100, 095005
Servidio, S., Matthaeus, W. H., Wan, M., et al. 2014, ApJ, 785, 56
Servidio, S., Valentini, F., Califano, F., & Veltri, P. 2012, PhRvL, 108, 045001
Servidio, S., Valentini, F., Perrone, D., et al. 2015, JPlPh, 81, 325810107
Shalchi, A. 2009, Nonlinear Cosmic Ray Diffusion Theories, Vol. 362 (Berlin: Springer)
Shay, M. A., Haggerty, C. C., Phan, T. D., et al. 2014, PhPl, 21, 122902
Shebalin, J. V. 1996, JPlPh, 56, 419
Sorriso-Valvo, L., Carbone, F., Perri, S., et al. 2018a, SoPh, 293, 10
Sorriso-Valvo, L., Perrone, D., Pezzi, O., et al. 2018b, JPlPh, 84, 725840201
Stribling, T., & Matthaeus, W. H. 1990, PhFlB, 2, 1979
Taylor, M. A., Kurien, S., & Eyink, G. L. 2003, PhRvE, 68, 026310
Vafin, S., Riazantseva, M., & Pohl, M. 2019, ApJL, 871, L11
Verma, M. K., Ayyer, A., & Chandra, A. V. 2005, PhPl, 12, 082307
Wan, M., Matthaeus, W. H., Karimabadi, H., et al. 2012, PhRvL, 109, 195001
Wan, M., Matthaeus, W. H., Roytershteyn, V., et al. 2015, PhRvL, 114, 175002
Wan, M., Oughton, S., Servidio, S., & Matthaeus, W. H. 2012, JFM, 697, 296
Wang, J., Yang, Y., Shi, Y., et al. 2013, PhRvL, 110, 214505
Yang, Y., Matthaeus, W. H., Parashar, T. N., et al. 2017a, PhRvE, 95, 061201
Yang, Y., Matthaeus, W. H., Parashar, T. N., et al. 2017b, PhPl, 24, 072306
Yang, Y., Shi, Y., Wan, M., Matthaeus, W. H., & Chen, S. 2016, PhRvE, 93, 061102
Yang, Y., Wan, M., Matthaeus, W. H., et al. 2019, MNRAS, 482, 4933
Zank, G. P., le Roux, J. A., Webb, G. M., Dosch, A., & Khabarova, O. 2014, ApJ, 797, 28
Zank, G. P., & Matthaeus, W. H. 1991, PhFlA, 3, 69
Zank, G. P., & Matthaeus, W. H. 1993, PhFlA, 5, 257
Zank, G. P., Matthaeus, W. H., & Smith, C. W. 1996, JGR, 101, 17093
Zeiler, A., Biskamp, D., Drake, J. F., et al. 2002, JGRA, 107, 1230
Zenitani, S., Hesse, M., Klimas, A., & Kuznetsova, M. 2011, PhRvL, 106, 195003